applied sciences

MDPI

Article

Initial Costate Approximation for Rapid Orbit Raising with Very Low Propulsive Acceleration

Alessandro A. Quarta

Department of Civil and Industrial Engineering, University of Pisa, I-56122 Pisa, Italy; alessandro.antonio.quarta@unipi.it

Abstract: The transfer between two circular, coplanar Keplerian orbits of a spacecraft equipped with a continuous thrust propulsion system is usually studied in an optimal framework by maximizing a given performance index. Using an indirect approach, the optimal trajectory and the maximum value of the performance index are obtained by numerically solving a two-point boundary value problem (TPBVP). In this context, the computation time required by the numerical solution of the TPBVP depends on the guess of unknown initial costates. The aim of this paper is to describe an analytical procedure to accurately approximate the initial costate variables in a coplanar, circle-to-circle, minimum-time transfer. In particular, this method considers a freely steerable propulsive acceleration vector, whose magnitude varies over a finite range with a sufficiently low maximum value. The effectiveness of the analytical method is tested in a set of both geocentric and heliocentric (simplified) mission scenarios, which model the classical LEO-GEO or interplanetary transfers toward Venus, Mars, Jupiter, and comet 29P/Schwassmann–Wachmann 1.

Keywords: continuous thrust propulsion system; circle-to-circle orbit transfer; trajectory optimization; optimal control problem; costate estimation

Citation: Quarta, A.A. Initial Costate Approximation for Rapid Orbit Raising with Very Low Propulsive Acceleration. *Appl. Sci.* **2024**, *14*, 1124. https://doi.org/10.3390/app14031124

Academic Editor: Cristian De Santis

Received: 18 December 2023
Revised: 5 January 2024
Accepted: 26 January 2024
Published: 29 January 2024

1. Introduction

The transfer between two circular, coplanar Keplerian orbits of a spacecraft equipped with a continuous thrust propulsion system is a classic astrodynamics problem [1] that is typically solved in an optimal framework by maximizing (or minimizing) a given scalar performance index as, for example, the propellant consumption or the total flight time. In this context, the optimization procedure described in the fundamental textbook by Bryson and Ho [2] is a typical example.

In fact, when the optimization problem is approached using the well-known indirect method [3,4], i.e., a method based on the classical theory of the calculus of variations [5], the solution requires the evaluation of the initial value of a set of costate variables, which is usually obtained by numerically solving a two-point boundary value problem (TPBVP). The computation time required by the numerical solution (and also by the convergence of the entire procedure) of the TPBVP associated with the optimization procedure is strongly dependent on the guess of unknown initial costates [6,7].

The purpose of this paper is to propose an analytical procedure to accurately approximate the initial costate variables in a coplanar, circle-to-circle minimum-time transfer, in order to initialize the numerical procedure that solves the TPBVP with an initial guess that is close to the actual solution. In particular, this paper considers a mission scenario in which the thrust vector is freely steerable during flight, and the magnitude of the propulsive acceleration varies over a finite range. The proposed procedure, which is consistent with the results from the classical literature [8–10], is suitable for the case of a propulsive acceleration vector with a low (or very low) maximum magnitude. In this scenario, the minimum-time transfer trajectory can be approximated through a tight spiral [11,12], and

some characteristics of the spacecraft osculating orbit can be described in an analytical (simple) form.

The proposed procedure is used here to analyze the optimal transfer in a set of both heliocentric and geocentric mission scenarios, as a function of the propulsive acceleration maximum magnitude. In particular, optimal circle-to-circle (rapid) spacecraft trajectories are studied in a classical LEO-GEO transfer and in a rendezvous mission towards Venus, Mars, Jupiter, and comet 29P/Schwassmann–Wachmann 1. Finally, the method discussed in this paper can also be used to rapidly obtain a set of accurate information about the optimal transfer trajectory in order to initialize more refined (trajectory) design procedures, such as those recently proposed by Huang et al. [13].

A natural extension of the method proposed in this work is to consider the dynamics of a spacecraft, which include the change in mass due to propellant consumption. This important aspect of the thrust vector model introduces a further parameter in the (optimal) design of the mission, namely the specific impulse, the value of which influences the overall transfer performance. On the other hand, the proposed method can be adapted to a scenario based on the use of a propellantless propulsion system such as, for example, a scenario involving a photonic solar sail [14,15] or Janhunen's Electric Solar Wind Sail [16,17].

2. Mathematical Preliminaries

Consider a two-dimensional scenario in which a spacecraft S initially (time instant $t = t_0 \triangleq 0$) covers a circular, Keplerian orbit of assigned radius r_0 around a primary body of gravitational parameter μ. The spacecraft is equipped with a continuous-thrust propulsion system which gives a freely steerable thrust vector and a propulsive acceleration $\boldsymbol{a}_p$ whose magnitude a_p ranges in the interval $[0, a_m]$, where $a_m > 0$ is the maximum (finite) value of a_p. The continuous propulsive acceleration induced by the primary propulsion system is used to transfer the spacecraft to a circular, coplanar, target orbit of assigned radius $r_f \neq r_0$ by minimizing the required flight time $\Delta t = t_f - t_0 \equiv t_f$, where $t_f > t_0$ is the final time instant. In other terms, the spacecraft transfer mission coincides with a minimum-time, circle-to-circle orbit raising if $r_f > r_0$, or orbit lowering when $r_f < r_0$. Bearing in mind the symmetry of the transfer problem, introduce a classical polar reference frame $\mathcal{T}(O; r, \theta)$ with the origin in the primary body center-of-mass O, in which r is the O-S distance and θ is the polar angle measured from the O-S line at the initial time instant. The polar reference frame $\mathcal{T}$ is sketched in Figure 1, where $\hat{\boldsymbol{i}}_r$ (or $\hat{\boldsymbol{i}}_\theta$) is the radial (or transverse) unit vector.

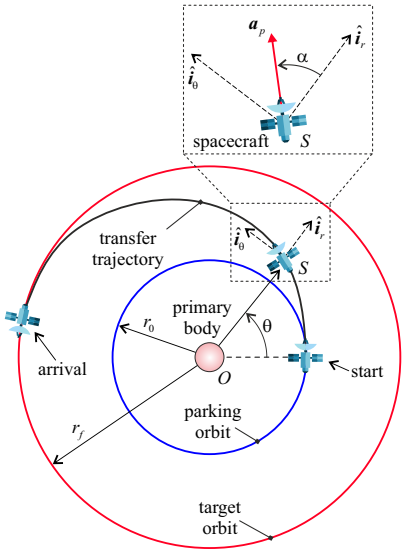

Figure 1. Polar reference frame $\mathcal{T}(O; r, \theta)$ with origin in the primary body center-of-mass and spacecraft propulsive acceleration vector $\boldsymbol{a}_p$. Blue line → circular parking orbit; red line → circular target orbit; black line → spacecraft optimal transfer trajectory.

In Figure 1, the direction of the spacecraft propulsive acceleration vector is identified by the thrust angle $\alpha \in [-\pi, \pi]$ rad, which is defined as the angle (measured counterclockwise into the plane of the circular parking orbit) between the *O*-*S* line and the direction of $\boldsymbol{a}_p$. Accordingly, the propulsive acceleration vector can be written as a function of the (control) angle α as

$$\boldsymbol{a}_p = a_p \cos\alpha \, \hat{\boldsymbol{i}}_r + a_p \sin\alpha \, \hat{\boldsymbol{i}}_\theta \tag{1}$$

so that the polar form of the spacecraft equations of motion are the well-known

$$\dot{r} = u \quad , \quad \dot{\theta} = \frac{v}{r} \quad , \quad \dot{u} = -\frac{\mu}{r^2} + \frac{v^2}{r} + a_p \cos\alpha \quad , \quad \dot{v} = -\frac{u\,v}{r} + a_p \sin\alpha, \tag{2}$$

where u (or v) is the radial (or transverse) component of the spacecraft velocity. The system of differential Equation (2) is completed by the 4 initial conditions that model the spacecraft traveling in the circular parking orbit, viz.

$$r(t_0) = r_0 \quad , \quad \theta(t_0) = 0 \quad , \quad u(t_0) = 0 \quad , \quad v(t_0) = \sqrt{\frac{\mu}{r_0}} \tag{3}$$

If the final value of the spacecraft polar angle $\theta(t_f)$ is unconstrained, the conditions for a circle-to-circle orbit transfer give the following 3 scalar constraints at the final time instant

$$r(t_f) = r_f \quad , \quad u(t_f) = 0 \quad , \quad v(t_f) = \sqrt{\frac{\mu}{r_f}} \tag{4}$$

The spacecraft equations of motion (2) and the boundary constraints given by Equations (3) and (4) can be rewritten more conveniently in a dimensionless form by introducing the (dimensionless) variables

$$\tilde{r} \triangleq \frac{r}{r_0} \quad , \quad \tilde{u} \triangleq \frac{u}{\sqrt{\mu/r_0}} \quad , \quad \tilde{v} \triangleq \frac{v}{\sqrt{\mu/r_0}} \quad , \quad \tilde{t} \triangleq \frac{t}{\sqrt{r_0^3/\mu}} \quad , \quad \tilde{a}_p \triangleq \frac{a_p}{\mu/r_0^2} \tag{5}$$

so that Equation (2) becomes

$$\tilde{r}' = \tilde{u} \quad , \quad \theta' = \frac{\tilde{v}}{\tilde{r}} \quad , \quad u' = -\frac{1}{\tilde{r}^2} + \frac{\tilde{v}^2}{\tilde{r}} + \tilde{a}_p \cos\alpha \quad , \quad \tilde{v}' = -\frac{\tilde{u}\,\tilde{v}}{\tilde{r}} + \tilde{a}_p \sin\alpha \tag{6}$$

where the prime symbol indicates the derivative with respect to the dimensionless time $\tilde{t}$. Accordingly, the boundary conditions written in Equations (3) and (4) become

$$\tilde{r}(\tilde{t}_0) = 1 \quad , \quad \theta(\tilde{t}_0) = 0 \quad , \quad \tilde{u}(\tilde{t}_0) = 0 \quad , \quad \tilde{v}(\tilde{t}_0) = 1 \tag{7}$$

and

$$\tilde{r}(\tilde{t}_f) = \tilde{r}_f \quad , \quad \tilde{u}(\tilde{t}_f) = 0 \quad , \quad \tilde{v}(\tilde{t}_f) = \frac{1}{\sqrt{\tilde{r}_f}} \tag{8}$$

in which $\tilde{r}_f$ is the dimensionless target radius, and $\tilde{t}_f$ is the dimensionless flight time to be minimized through a suitable selection of the spacecraft controls $\{\tilde{a}_p, \alpha\}$. Note that Equations (6)–(8) are independent of both the actual value of the primary body gravitational parameter and the radius of the circular parking orbit. The optimization of the spacecraft transfer trajectory, i.e., the calculation of the time variation in both the thrust angle α and the propulsive acceleration (dimensionless) magnitude $\tilde{a}_p$ that minimizes the flight time, is described in the next section.

3. Trajectory Optimization Using an Indirect Method

The circle-to-circle, minimum-time continuous-thrust orbit transfer optimization is studied using an indirect method, that is, a method based on the classical calculus of

variations. In this context, and keeping in mind the mathematical model described in references [2,5], the dimensionless performance index J to be maximized is written as

$$J \triangleq -\Delta t \equiv -\tilde{t}_f \tag{9}$$

while the (dimensionless) Hamiltonian function $\mathcal{H}$ is given, according to Equation (6), by

$$\mathcal{H} = \lambda_{\tilde{r}}\,\tilde{u} + \lambda_\theta\,\frac{\tilde{v}}{\tilde{r}} + \lambda_{\tilde{u}}\left(\frac{\tilde{v}^2}{\tilde{r}} - \frac{1}{\tilde{r}^2}\right) - \lambda_{\tilde{v}}\,\frac{\tilde{u}\,\tilde{v}}{\tilde{r}} + \mathcal{H}_c \tag{10}$$

where $\{\lambda_{\tilde{r}},\, \lambda_\theta,\, \lambda_{\tilde{u}},\, \lambda_{\tilde{v}}\}$ are the dimensionless costates, and $\mathcal{H}_c$ is the part of the Hamiltonian function that explicitly depends on the two control terms $\{\tilde{a}_p,\, \alpha\}$, viz.

$$\mathcal{H}_c \triangleq \tilde{a}_p\,(\lambda_{\tilde{u}}\,\cos\alpha + \lambda_{\tilde{v}}\,\sin\alpha) \tag{11}$$

The optimal value of the controls $\{\tilde{a}_p,\, \alpha\}$ is obtained by using Pontryagin's maximum principle [18], i.e., by maximizing (at any time instant) the function $\mathcal{H}_c$ defined in the previous equation. More precisely, bearing in mind that $\mathcal{H}_c$ is linear in $\tilde{a}_p$ and that the thrust vector direction (i.e., the value of α) is unconstrained, the optimal control law is simply given by

$$\tilde{a}_p = \tilde{a}_m \triangleq \frac{a_m}{\mu/r_0^2} \quad , \quad \cos\alpha = \frac{\lambda_{\tilde{u}}}{\sqrt{\lambda_{\tilde{u}}^2 + \lambda_{\tilde{v}}^2}} \quad , \quad \sin\alpha = \frac{\lambda_{\tilde{v}}}{\sqrt{\lambda_{\tilde{u}}^2 + \lambda_{\tilde{v}}^2}} \tag{12}$$

where $\tilde{a}_m$ represents the dimensionless form of the maximum propulsive acceleration magnitude a_m. Note that, as expected, the control law reassumed in Equation (12) is consistent with the result presented in reference [2]. In particular, the first of Equation (12) indicates that the rapid transfer is obtained by selecting the maximum value of a_p (i.e., no coasting arcs appear in the optimal transfer trajectory), while the last two equations indicate that the optimal thrust direction coincides with the classical Lawden's primer vector direction [19].

In this context, the time variation in the optimal thrust angle is obtained, through Equation (12), by (numerically) solving the Euler–Lagrange equations [2,5], which give the $\tilde{t}$-derivative of the four costates $\{\lambda_{\tilde{r}},\, \lambda_\theta,\, \lambda_{\tilde{u}},\, \lambda_{\tilde{v}}\}$ as

$$\lambda'_{\tilde{r}} = -\frac{\partial\mathcal{H}}{\partial\tilde{r}} = \frac{\tilde{v}(\lambda_\theta - \lambda_{\tilde{v}}\,\tilde{u} + \lambda_{\tilde{u}}\,\tilde{v})}{\tilde{r}^2} - \frac{2\,\lambda_{\tilde{u}}}{\tilde{r}^3} \tag{13}$$

$$\lambda'_\theta = -\frac{\partial\mathcal{H}}{\partial\theta} = 0 \tag{14}$$

$$\lambda'_{\tilde{u}} = -\frac{\partial\mathcal{H}}{\partial\tilde{u}} = \frac{\lambda_{\tilde{v}}\,\tilde{v}}{\tilde{r}} - \lambda_{\tilde{r}} \tag{15}$$

$$\lambda'_{\tilde{v}} = -\frac{\partial\mathcal{H}}{\partial\tilde{v}} = \frac{\lambda_{\tilde{v}}\,\tilde{u} - \lambda_\theta - 2\,\lambda_{\tilde{u}}\,\tilde{v}}{\tilde{r}} \tag{16}$$

The expression of the Hamiltonian function is also used to evaluate the transversality condition [2], which in this case gives the following two scalar constraints at the final time

$$\lambda_\theta(\tilde{t}_f) = 0 \quad , \quad \mathcal{H}(\tilde{t}_f) = 1 \tag{17}$$

In particular, taking Equation (14) into account, we obtain that

$$\lambda_\theta = 0 \tag{18}$$

during the transfer, so Equations (13) and (16) are simplified as

$$\lambda'_{\tilde{r}} = \frac{\tilde{v}(\lambda_{\tilde{u}}\,\tilde{v} - \lambda_{\tilde{v}}\,\tilde{u})}{\tilde{r}^2} - \frac{2\,\lambda_{\tilde{u}}}{\tilde{r}^3} \tag{19}$$

$$\lambda'_{\tilde{v}} = \frac{\lambda_{\tilde{v}}\,\tilde{u} - 2\,\lambda_{\tilde{u}}\,\tilde{v}}{\tilde{r}} \tag{20}$$

On the other hand, observing that the dimensionless time $\tilde{t}$ does not compare explicitly in the expression of the Hamiltonian function given by Equation (10), one has that the value of $\mathcal{H}$ is a constant of motion [2]. Accordingly, the second of Equation (17) can be rewritten as

$$\mathcal{H}(\tilde{t}_0) = 1 \tag{21}$$

Bearing in mind Equations (10) and (11), the optimal control law given by Equation (12), the initial conditions reassumed in Equation (7), and the expression of λ_θ given by Equation (18), the previous equation gives the following constraint at the initial time instant

$$\tilde{a}_m \sqrt{\lambda^2_{\tilde{u}}(\tilde{t}_0) + \lambda^2_{\tilde{v}}(\tilde{t}_0)} = 1 \tag{22}$$

where $\lambda_{\tilde{u}}(\tilde{t}_0)$ (or $\lambda_{\tilde{v}}(\tilde{t}_0)$) is the initial value of the dimensionless costate $\lambda_{\tilde{u}}$ (or $\lambda_{\tilde{v}}$), which is one of the unknowns of the associated TPBVP. The previous equation states that the point $\{\lambda_{\tilde{u}}(\tilde{t}_0),\ \lambda_{\tilde{v}}(\tilde{t}_0)\}$ lies on a circle of radius equal to $1/\tilde{a}_m$, as sketched in Figure 2, where the auxiliary angle $\delta \in [-\pi/2,\ \pi/2]$ rad is introduced.

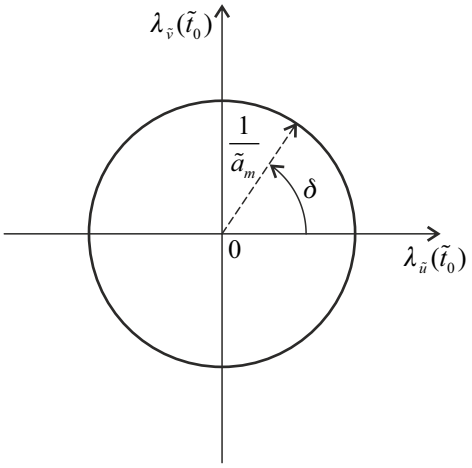

Figure 2. Variation in $\lambda_{\tilde{u}}(\tilde{t}_0)$ and $\lambda_{\tilde{v}}(\tilde{t}_0)$ with the auxiliary angle δ; see also Equation (22).

Accordingly, Equation (22) and Figure 2 allow the pair $\{\lambda_{\tilde{u}}(\tilde{t}_0),\ \lambda_{\tilde{v}}(\tilde{t}_0)\}$ to be calculated as a function of the single (geometric) dimensionless variable δ as

$$\lambda_{\tilde{u}}(\tilde{t}_0) = \frac{\cos\delta}{\tilde{a}_m} \quad , \quad \lambda_{\tilde{v}}(\tilde{t}_0) = \frac{\sin\delta}{\tilde{a}_m} \tag{23}$$

Note that the auxiliary angle δ coincides with the initial value of the thrust angle, that is, $\delta \equiv \alpha(\tilde{t}_0)$; compare Equation (12) with Equation (23).

The TPBVP associated with the optimization problem is then formed by the 7 differential equations, Equations (6), (15), (19) and (20), the 4 initial conditions (7), and the 3 final conditions (8). In particular, the solution of the TPBVP requires the final time $\tilde{t}_f$, the auxiliary angle δ, and the initial costate $\lambda_{\tilde{r}}(\tilde{t}_0)$ to be numerically calculated by enforcing the (final) boundary constraints of Equation (8). However, the convergence of the procedure used to solve the TPBVP, which is usually based on standard numerical methods as the single or multiple shooting procedure [20], depends on the appropriate selection

of a guessed value of the triplet $\{\tilde{t}_f, \delta, \lambda_{\tilde{r}}(\tilde{t}_0)\}$. In this respect, the next section describes an analytical method for selecting a triplet $\{\tilde{t}_f, \delta, \lambda_{\tilde{r}}(\tilde{t}_0)\}$ sufficiently close to the effective value that resolves the TPBVP.

4. Analytical Method for the Approximation of Flight Time and Initial Costates

In this section, an analytical approximation of the three unknowns $\{\tilde{t}_f, \delta, \lambda_{\tilde{r}}(\tilde{t}_0)\}$, that is, the flight time and the initial costates, is detailed. In particular, the proposed procedure can be applied when $\tilde{a}_m \ll 1$. This is the important case of a spacecraft equipped with a low-performance (or a very low-performance) propulsion system, which gives a propulsive acceleration whose maximum value is only a (small) fraction of the gravitational acceleration μ/r_0^2 along the circular parking orbit. In this scenario, the total flight time is usually very high (a few dozen, or even hundreds, of parking orbit periods), and the knowledge of an accurate guess of the triplet $\{\tilde{t}_f, \delta, \lambda_{\tilde{r}}(\tilde{t}_0)\}$ is a crucial point in reducing the computation time required to solve the associated TPBVP. In this context, the last part of this section describes a method that can be used to rapidly estimate, as a function of the mission scenario characteristics in terms of $\tilde{a}_m$ and $\tilde{r}_f$, the maximum value of $\tilde{a}_m$ compatible with the proposed, analytical approximate procedure.

In fact, the proposed method is based on the observation that, when $\tilde{a}_m \ll 1$, the optimal transfer trajectory resembles a tight spiral, i.e., the value of the spacecraft (dimensionless) radial acceleration u' is nearly zero during the entire transfer between the two (coplanar) circular orbits. In this case, the numerical simulations indicate that the direction of the propulsive acceleration vector is substantially transverse (i.e., the radial component of $\boldsymbol{a}_p$ is very low when compared with the transverse component) so that the thrust angle α is substantially a constant of motion with

$$\alpha \simeq \begin{cases} \dfrac{\pi}{2}\,\text{rad} & \text{if} \quad \tilde{r}_f > 1 \\ -\dfrac{\pi}{2}\,\text{rad} & \text{if} \quad \tilde{r}_f < 1 \end{cases} \qquad \text{for} \quad t \in [t_0,\, t_f] \tag{24}$$

Note that the latter equation can be rewritten in a compact form as

$$\alpha \simeq \text{sign}\left(\tilde{r}_f - 1\right) \frac{\pi}{2}\,\text{rad} \qquad \text{for} \quad t \in [t_0,\, t_f] \tag{25}$$

where $\text{sign}(\square) \in \{-1,\, 1\}$ is the signum function. Accordingly, the value of the first of the three unknowns, i.e., the auxiliary angle δ which coincides with the initial value of the thrust angle, is approximated through the simple equation

$$\delta \simeq \text{sign}\left(\tilde{r}_f - 1\right) \frac{\pi}{2}\,\text{rad} \tag{26}$$

Recall that the value of δ allows the two initial costates $\lambda_{\tilde{u}}(\tilde{t}_0)$ and $\lambda_{\tilde{v}}(\tilde{t}_0)$ to be calculated using Equation (23) as a function of the maximum magnitude of the dimensionless propulsive acceleration $\tilde{a}_m$.

The second unknown, i.e., the value of the dimensionless flight time $\tilde{t}_f$, can be approximated using a simplified form of the spacecraft dynamics. In fact, bearing in mind that $\tilde{a}_p = \tilde{a}_m$ during the entire transfer (see first of Equation (12)), the last of Equation (6) gives

$$\tilde{h}' = \tilde{a}_m\, \text{sign}\left(\tilde{r}_f - 1\right) \tilde{r} \tag{27}$$

where $\tilde{h} = \tilde{r}\,\tilde{v}$ is the dimensionless magnitude of the spacecraft-specific angular momentum vector $\boldsymbol{h}$, i.e., $\tilde{h} = \|\boldsymbol{h}\| / \sqrt{\mu\, r_0}$. Furthermore, according to the third of Equation (6), when $\cos\alpha \simeq 0$ and $u' \simeq 0$, the dimensionless magnitude $\tilde{h}$ can be approximated as

$$\tilde{h} = \tilde{r}\,\tilde{v} \simeq \sqrt{\tilde{r}} \tag{28}$$

so that, with the aid of the previous equation, one has $\tilde{r} \simeq \tilde{h}^2$, and Equation (27) can be easily solved to give an analytical approximation of the dimensionless (minimum) flight time

$$\tilde{t}_f = \frac{1}{\tilde{a}_m \operatorname{sign}\left(\tilde{r}_f - 1\right)} \left(1 - \frac{1}{\sqrt{\tilde{r}_f}}\right) \tag{29}$$

Note that the expression of the minimum flight time given by Equation (29) is consistent with the classical result obtained by Alfano et al. [8–10] using the elegant concept of the accumulated velocity change. The same concept has also been used by the author to evaluate the optimal performance of a solar-sail-based spacecraft in a typical heliocentric mission scenario [21,22].

The last of the three unknowns required to initialize the associated TPBVP, i.e., the value of the initial costate $\lambda_{\tilde{r}}(\tilde{t}_0)$, can be approximated by firstly enforcing in Equation (15) the initial conditions given by Equation (7), viz.

$$\lambda'_{\tilde{u}}(\tilde{t}_0) = \lambda_{\tilde{v}}(\tilde{t}_0) - \lambda_{\tilde{r}}(\tilde{t}_0) \tag{30}$$

Now, according to Equations (23) and (26), the value of $\lambda_{\tilde{v}}(\tilde{t}_0)$ is given by

$$\lambda_{\tilde{v}}(\tilde{t}_0) = \frac{\operatorname{sign}\left(\tilde{r}_f - 1\right)}{\tilde{a}_m} \tag{31}$$

while $\lambda_{\tilde{u}} \simeq 0$ is substantially constant during the transfer (remember that the direction of the propulsive acceleration vector is essentially transverse during the transfer) so that

$$\lambda'_{\tilde{u}}(\tilde{t}_0) = 0 \tag{32}$$

The value of the last unknown $\lambda_{\tilde{r}}(\tilde{t}_0)$ is then obtained by substituting Equations (31) and (32) in Equation (30), and the result is

$$\lambda_{\tilde{r}}(\tilde{t}_0) = \frac{\operatorname{sign}\left(\tilde{r}_f - 1\right)}{\tilde{a}_m} \tag{33}$$

or, equivalently, $\lambda_{\tilde{r}}(\tilde{t}_0) = \lambda_{\tilde{v}}(\tilde{t}_0)$.

Maximum Value of $\tilde{a}_m$ Compatible with the Proposed Method

The approximation of the triplet $\{\tilde{t}_f, \delta, \lambda_{\tilde{r}}(\tilde{t}_0)\}$ given by Equations (26), (29) and (33) is accurate when the optimal transfer trajectory resembles a tight spiral so that the osculating orbit is substantially circular and the radial component of the spacecraft acceleration $\tilde{u}'$ is nearly zero. The latter is, in fact, a scenario analyzed in detail by Alfano et al. [8]. In particular, reference [8] discusses that the accumulated velocity change ΔV defined as

$$\Delta V = \int_{t_0}^{t_f} a_p \, \mathrm{d}t \tag{34}$$

in this specific case (i.e., when the osculating orbit is nearly circular) can be approximated through a very simple equation that depends on the radius of both the parking and the target orbit, viz.

$$\Delta V = a_m \, t_f \simeq \begin{cases} \sqrt{\dfrac{\mu}{r_0}} - \sqrt{\dfrac{\mu}{r_f}} & \text{if} \quad r_f > r_0 \\ \sqrt{\dfrac{\mu}{r_f}} - \sqrt{\dfrac{\mu}{r_0}} & \text{if} \quad r_f < r_0 \end{cases} \tag{35}$$

In particular, the latter equation indicates that the accumulated velocity change ΔV coincides with the difference between the spacecraft velocity along the target and the

parking orbit. Note also that Equation (35) is consistent with the model proposed in this paper; see, for instance, Equation (29).

Using the results detailed in reference [8] in terms of plots of the accumulated velocity change ΔV as a function of the characteristics of the propulsion system a_m and the radius of the target circular orbit, we obtain that Equation (35) holds (i.e., the approximation of an osculating nearly circular orbit is valid) when the spacecraft completes, during the transfer, a number n of revolutions around the primary body at least equal to 5. However, extensive numerical simulations indicate that the method proposed in this work still gives an accurate approximation of the initial costates when $n \geq 2$. In fact, as underlined by Alfano et al. [8], when $n < 2$, the intensity of the propulsive acceleration becomes comparable to the gravitational acceleration of the primary body, and the shape of the transfer trajectory (i.e., the characteristics of the spacecraft osculating orbit) is substantially influenced by the thrust vector magnitude and direction.

The value of n can be estimated using an analytical expression obtained through the combination of Equations (6), (25), and (28). Indeed, assuming $\tilde{a}_p \, \sin\alpha \simeq \tilde{a}_m \, \mathrm{sign}\left(\tilde{r}_f - 1\right)$ during the transfer, with the aid of Equation (28), the second and the last of Equation (6) give

$$\frac{\mathrm{d}\theta}{\mathrm{d}\tilde{h}} = \frac{\tilde{h}}{\tilde{a}_m \, \mathrm{sign}\left(\tilde{r}_f - 1\right) \tilde{r}^3} \equiv \frac{1}{\tilde{a}_m \, \mathrm{sign}\left(\tilde{r}_f - 1\right) \tilde{h}^5} \tag{36}$$

which can be easily solved to obtain the final value of the spacecraft polar angle $\theta(\tilde{t}_f)$ as a function of both the (dimensionless) maximum propulsive acceleration magnitude $\tilde{a}_m$ and the target orbit radius $\tilde{r}_f$, viz.

$$\theta(\tilde{t}_f) = \frac{1}{4 \, \tilde{a}_m \, \mathrm{sign}\left(\tilde{r}_f - 1\right)} \left(1 - \frac{1}{\tilde{r}_f^2}\right) \tag{37}$$

Accordingly, the value of n is obtained from the previous equation as

$$n = \mathrm{floor}\left[\frac{\theta(\tilde{t}_f)}{2\pi}\right] = \mathrm{floor}\left[\frac{1}{8 \, \pi \, \tilde{a}_m \, \mathrm{sign}\left(\tilde{r}_f - 1\right)} \left(1 - \frac{1}{\tilde{r}_f^2}\right)\right] \tag{38}$$

where floor$[\square]$ is the floor function [20].

Therefore, the procedure can be summarized as follows. For a given (dimensionless) value of the target orbit radius $\tilde{r}_f$ and the maximum propulsive acceleration magnitude $\tilde{a}_m$, the estimated number of complete revolutions during the transfer n is calculated through Equation (38). If the obtained value is $n \geq 2$, the proposed analytical method is valid, and the expression of the triplet $\{\tilde{t}_f, \delta, \lambda_{\tilde{r}}(\tilde{t}_0)\}$ given by Equations (26), (29), and (33) can be used to obtain a reasonable approximation of the actual values that resolve the associated TPBVP. Otherwise, the actual value of the unknown initial costates can be very different from those determined analytically. On the other hand, Equations (26), (29), and (33) can still be used to rapidly obtain a (very rough) guess to initialize the TPBVP numerical solution through standard methods [20].

5. Model Validation and Numerical Simulations

The proposed procedure was tested in a set of circle-to-circle orbit, two-dimensional transfers that model some typical heliocentric (in which the primary body is the Sun and $\mu = \mu_\odot = 132{,}712{,}439{,}935.5\,\mathrm{km}^3/\mathrm{s}^2$) and geocentric (in which the primary body is Earth and $\mu = \mu_\oplus = 398{,}600\,\mathrm{km}^3/\mathrm{s}^2$) mission scenarios.

In particular, regarding a potential heliocentric mission scenario, the initial parking orbit radius was set equal to 1 AU. In fact, the case of $r_0 = 1$ AU models the situation in which the spacecraft begins the heliocentric phase of a typical interplanetary transfer after escaping from Earth using a parabolic (escape) orbit. In this context, three different

(circular) target obits were considered; that is, three different values of r_f were used in the numerical simulations, namely (i) $r_f = r_{\varnothing} = 0.723$ AU, which models an Earth–Venus transfer; (ii) $r_f = r_{\male} = 1.524$ AU, which models an Earth–Mars transfer; and (iii) $r_f = r_{\jupiter} = 5.203$ AU, which models an Earth–Jupiter transfer. Accordingly, in this selected set of heliocentric mission scenarios, the dimensionless value of the target orbit radius is $\tilde{r}_f = r_f/r_0 = \{\tilde{r}_{\varnothing}, \tilde{r}_{\male}, \tilde{r}_{\jupiter}\} = \{0.723, 1.524, 5.203\}$. As regards the geocentric mission scenario, a classical (two-dimensional) LEO-GEO transfer is considered, in which the radius of the circular parking orbit is $r_0 = r_{\text{LEO}} = 6578$ km (i.e., a circular LEO of 200 km of altitude is assumed) and the target orbit has a radius $r_f = r_{\text{GEO}} = 42{,}164$ km. Therefore, in the geocentric case, the dimensionless value of the target orbit radius is $\tilde{r}_f = r_{\text{GEO}}/r_{\text{LEO}} \triangleq \tilde{r}_{\text{G}} \simeq 6.41$.

The number n of completed revolutions around the primary body, in the four proposed mission scenarios, can be calculated using Equation (38) as a function of the value of $\tilde{a}_m$. The function $n = n(\tilde{a}_m)$ is shown in Figure 3 when $\tilde{a}_m < 0.05$ and $\tilde{r}_f = \{\tilde{r}_{\varnothing}, \tilde{r}_{\male}, \tilde{r}_{\jupiter}, \tilde{r}_{\text{G}}\}$. In particular, the stepped curves in Figure 3 allow us to quickly estimate the maximum value of $\tilde{a}_m$ for which the proposed analytical approximation can be used to initialize the associated TPBVP. In fact, according to Figure 3, the condition $n \geq 2$ is met when (i) $\tilde{a}_m \leq 0.018$ in the Earth–Venus scenario; (ii) $\tilde{a}_m \leq 0.011$ in the Earth–Mars scenario; (iii) $\tilde{a}_m \leq 0.018$ in the Earth–Jupiter scenario; and (iv) $\tilde{a}_m \leq 0.019$ in the LEO-GEO scenario.

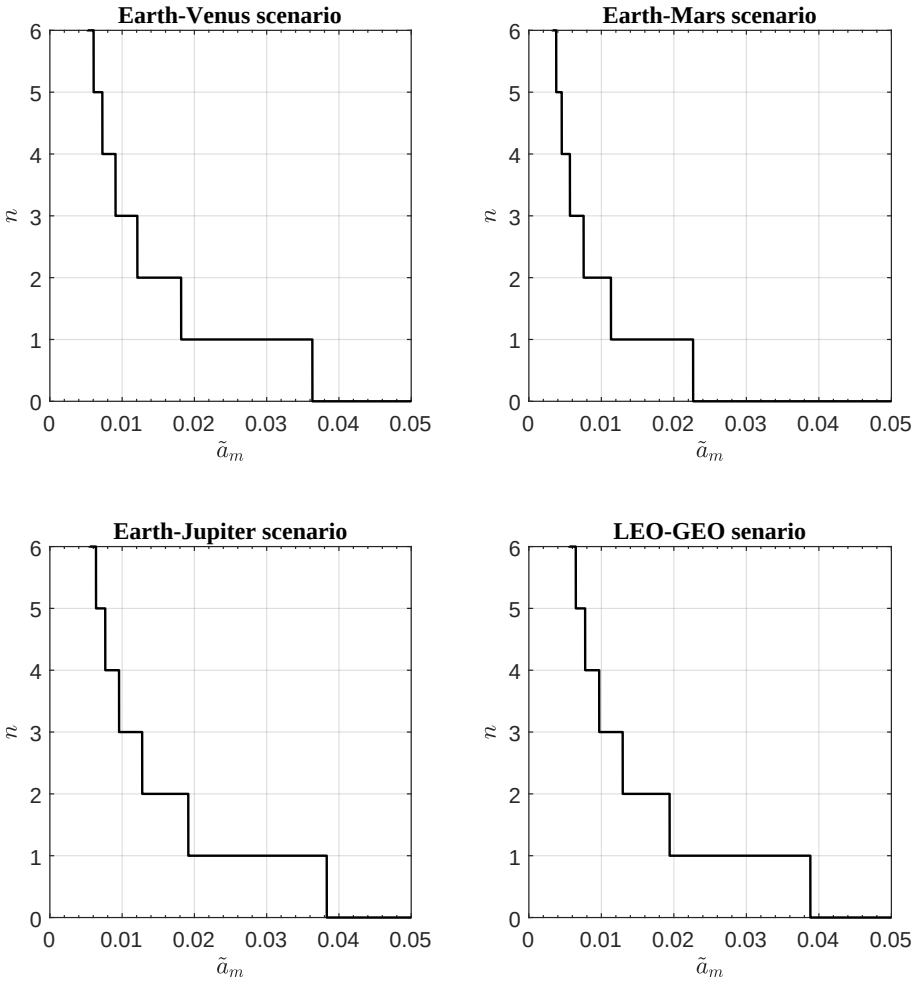

Figure 3. Number n of completed revolutions around the primary body in the four analyzed mission scenarios. The value of n is calculated using Equation (38).

As a result, the validity of the proposed method was tested by considering, for each mission scenario, about 20 values of $\tilde{a}_m$ ranging between 0.001 and 0.02 (with a step of 0.001).

For each value of $\tilde{a}_m$, the optimal (i.e., the rapid) transfer trajectory was calculated by solving the associated TPBVP using a single shooting method [20], which was initialized according to the expressions given by Equations (26), (29), and (33). In that context, the equations of motion (6) and the Euler–Lagrange equations (15), (19), and (20) were integrated in double precision using the Adams–Bashforth method [23] with an absolute and relative tolerance of 1×10^{-10}, while the tolerance on the convergence of the TPBVP was set to 1×10^{-8}. The solution of the numerical procedure gives the actual value of the triplet $\{\tilde{t}_f, \delta, \lambda_{\tilde{r}}(\tilde{t}_0)\}$, which was compared with the analytical approximation given by Equations (26), (29), and (33) by introducing the ratio $\{R_t, R_\delta, R_\lambda\}$ defined as

$$R_t \triangleq \frac{\tilde{t}_f\big|_{\text{an}}}{\tilde{t}_f\big|_{\text{num}}} \quad , \quad R_\delta \triangleq \frac{\delta|_{\text{an}}}{\delta|_{\text{num}}} \quad , \quad R_\lambda \triangleq \frac{\lambda_{\tilde{r}}(\tilde{t}_0)|_{\text{an}}}{\lambda_{\tilde{r}}(\tilde{t}_0)|_{\text{num}}} \tag{39}$$

where $\square|_{\text{an}}$ indicates the value of $\square$ calculated through the analytical approximation, while $\square|_{\text{num}}$ is the actual value of $\square$ (calculated numerically) that solves the TPBVP.

The results of the numerical simulations for the four exemplary mission scenarios are summarized in Tables 1–4 in terms of $\{\tilde{t}_f, \theta(\tilde{t}_f), n, R_t, R_\delta, R_\lambda\}$ as a function of $\tilde{a}_m$. In particular, as also explicitly indicated in the table captions, the values of $\{\tilde{t}_f, \theta(\tilde{t}_f)\}$ are the results of the numerical solutions of the associated TPBVP, the value of n is obtained analytically from Equation (38), and the three ratios $\{R_t, R_\delta, R_\lambda\}$ are calculated according to Equation (39). The last three columns in Tables 1–4 confirm that the analytical approximations proposed in this work are consistent with the actual (numerical) values of the unknown costates. Furthermore, the expression of n given by Equation (38) gives a very good approximation of the actual number of completed revolutions around the primary body during the transfer. Finally, the value of $R_t \simeq 1$ in all the transfers analyzed indicates that the expression of the flight time given by Equation (29) is well suited to rapidly calculate the minimum transfer time without solving (numerically) the optimization problem, especially for low propulsive acceleration magnitude.

Table 1. Earth–Venus transfer scenario: Simulations results and comparison with the analytical approximations. The values of $\{\tilde{t}_f, \theta(\tilde{t}_f)\}$ are obtained through the numerical solution of the TPBVP, while the values of $\{n, R_t, R_\delta, R_\lambda\}$ are calculated using Equations (38) and (39).

$\tilde{a}_m$	$\tilde{t}_f$	$\frac{\theta(\tilde{t}_f)}{2\pi \text{ rad}}$	n	R_t	R_δ	R_λ
0.0200	9.0891	1.8714	1	0.9685	1.0581	1.1168
0.0190	9.4517	1.9465	1	0.9804	1.0585	1.0574
0.0180	9.9729	2.0532	2	0.9808	1.0758	0.9234
0.0170	10.8329	2.2235	2	0.9560	1.1265	0.8450
0.0160	11.7170	2.4040	2	0.9391	1.1142	0.9875
0.0150	12.4297	2.5563	2	0.9443	1.0858	1.0846
0.0140	13.0835	2.6953	2	0.9612	1.0631	1.1242
0.0130	13.7920	2.8431	2	0.9820	1.0467	1.1058
0.0120	14.8073	3.0526	3	0.9909	1.0523	0.9464
0.0110	16.5729	3.4115	3	0.9658	1.0930	0.9863
0.0100	17.9887	3.7088	3	0.9787	1.0516	1.1049
0.0090	19.6685	4.0565	4	0.9946	1.0398	0.9561
0.0080	22.4148	4.6218	4	0.9818	1.0542	1.0761
0.0070	25.3971	5.2372	5	0.9903	1.0567	0.9097
0.0060	29.4209	6.0694	6	0.9974	1.0271	0.9640
0.0050	35.4514	7.3124	7	0.9933	1.0458	0.9449
0.0040	44.0759	9.0937	9	0.9986	1.0190	0.9683
0.0030	58.7415	12.1199	12	0.9991	1.0152	0.9707
0.0020	88.0827	18.1742	18	0.9994	1.0117	0.9749
0.0010	176.1164	36.3391	36	0.9997	1.0087	0.9886

Table 2. Earth–Mars transfer scenario: Simulations results and comparison with the analytical approximations. The values of $\{\tilde{t}_f, \theta(\tilde{t}_f)\}$ are obtained through the numerical solution of the TPBVP, while the values of $\{n, R_t, R_\delta, R_\lambda\}$ are calculated using Equations (38) and (39).

$\tilde{a}_m$	$\tilde{t}_f$	$\frac{\theta(\tilde{t}_f)}{2\pi \text{ rad}}$	n	R_t	R_δ	R_λ
0.0200	10.9517	1.2682	1	0.8673	1.1910	0.7537
0.0190	11.6424	1.3496	1	0.8587	1.2644	0.8702
0.0180	12.2842	1.4296	1	0.8591	1.2667	0.9959
0.0170	12.8860	1.5080	1	0.8671	1.2234	1.1081
0.0160	13.4678	1.5853	1	0.8815	1.1600	1.1941
0.0150	14.0555	1.6621	1	0.9010	1.0919	1.2475
0.0140	14.6830	1.7410	1	0.9241	1.0246	1.2647
0.0130	15.4023	1.8285	1	0.9487	0.9571	1.2329
0.0120	16.3349	1.9403	1	0.9691	0.8903	1.0959
0.0110	17.9448	2.1263	2	0.9623	0.9419	0.7580
0.0100	20.3405	2.4028	2	0.9339	1.2309	0.9414
0.0090	22.2409	2.6424	2	0.9490	1.1018	1.1919
0.0080	24.2123	2.8826	2	0.9807	0.9390	1.1466
0.0070	28.1388	3.3410	3	0.9644	1.1712	0.8674
0.0060	32.1339	3.8285	3	0.9852	0.9766	1.1567
0.0050	38.7875	4.6203	4	0.9795	1.0925	1.1234
0.0040	48.0039	5.7220	5	0.9893	1.0323	1.1320
0.0030	63.8465	7.6117	7	0.9917	1.0687	1.0770
0.0020	95.3378	11.3685	11	0.9962	1.0565	0.9492
0.0010	190.1195	22.6756	22	0.9992	1.0180	1.0346

Table 3. Earth–Jupiter transfer scenario: Simulations results and comparison with the analytical approximations. The values of $\{\tilde{t}_f, \theta(\tilde{t}_f)\}$ are obtained through the numerical solution of the TPBVP, while the values of $\{n, R_t, R_\delta, R_\lambda\}$ are calculated using Equations (38) and (39).

$\tilde{a}_m$	$\tilde{t}_f$	$\frac{\theta(\tilde{t}_f)}{2\pi \text{ rad}}$	n	R_t	R_δ	R_λ
0.0200	36.7978	2.1084	1	0.7631	0.9835	0.8611
0.0190	38.5040	2.2135	2	0.7677	1.0476	0.8846
0.0180	40.3135	2.3341	2	0.7739	1.0934	0.9699
0.0170	42.1620	2.4689	2	0.7835	1.0772	1.0898
0.0160	44.0699	2.6120	2	0.7965	1.0062	1.1607
0.0150	46.1890	2.7608	2	0.8106	0.9361	1.1156
0.0140	48.7870	2.9285	2	0.8222	0.9152	0.9748
0.0130	52.1409	3.1349	2	0.8285	0.9915	0.8766
0.0120	56.0312	3.3943	3	0.8352	1.0867	1.0070
0.0110	59.9808	3.6892	3	0.8512	0.9770	1.1402
0.0100	64.9083	4.0151	3	0.8652	0.9377	0.9266
0.0090	71.5448	4.4562	4	0.8722	1.0758	1.0440
0.0080	78.8197	4.9711	4	0.8906	0.9305	0.9639
0.0070	88.9817	5.6716	5	0.9016	0.9964	1.1259
0.0060	102.3114	6.5813	6	0.9149	1.0374	1.1005
0.0050	120.4783	7.8453	7	0.9323	0.9445	1.0610
0.0040	148.2645	9.7628	9	0.9470	0.9719	1.0965
0.0030	194.3215	12.9393	12	0.9633	0.9441	1.0087
0.0020	287.0700	19.3137	19	0.9782	1.0326	0.9412
0.0010	565.6686	38.4400	38	0.9928	1.0356	0.9898

Table 4. LEO-GEO transfer scenario: Simulations results and comparison with the analytical approximations. The values of $\{\tilde{t}_f, \theta(\tilde{t}_f)\}$ are obtained through the numerical solution of the TPBVP, while the values of $\{n, R_t, R_\delta, R_\lambda\}$ are calculated using Equations (38) and (39).

$\tilde{a}_m$	$\tilde{t}_f$	$\frac{\theta(\tilde{t}_f)}{2\pi \text{ rad}}$	n	R_t	R_δ	R_λ
0.0200	41.6750	2.1459	1	0.7255	1.0164	0.8756
0.0190	43.5002	2.2535	2	0.7317	1.0694	0.9258
0.0180	45.4088	2.3757	2	0.7398	1.0868	1.0236
0.0170	47.3755	2.5098	2	0.7508	1.0456	1.1223
0.0160	49.4705	2.6504	2	0.7640	0.9756	1.1454
0.0150	51.8737	2.8005	2	0.7772	0.9245	1.0635
0.0140	54.8463	2.9741	2	0.7875	0.9333	0.9311
0.0130	58.5463	3.1874	2	0.7945	1.0272	0.8961
0.0120	62.6263	3.4505	3	0.8047	1.0680	1.0621
0.0110	66.9178	3.7412	3	0.8215	0.9508	1.1021
0.0100	72.5172	4.0775	3	0.8339	0.9706	0.9016
0.0090	79.5200	4.5259	4	0.8450	1.0443	1.0925
0.0080	87.6519	5.0452	4	0.8624	0.9579	0.9201
0.0070	98.4573	5.7500	5	0.8774	0.9610	1.0929
0.0060	112.8880	6.6749	6	0.8928	0.9912	1.1075
0.0050	132.7177	7.9526	7	0.9113	0.9427	0.9820
0.0040	162.6657	9.8933	9	0.9294	0.9459	1.0210
0.0030	212.5907	13.1174	12	0.9482	0.9780	0.9292
0.0020	312.3595	19.5955	19	0.9680	1.0278	1.0631
0.0010	611.7156	38.9691	38	0.9886	0.9652	1.0002

Case Study: Transfer towards Comet 29P/Schwassmann–Wachmann 1

The proposed method is now used to rapidly solve the TPBVP associated with the (heliocentric) minimum-time transfer towards comet 29P/Schwassmann–Wachmann 1 [24–27]. The latter was very recently considered by the author [28] as a potential target for a solar-sail-based (rendezvous) interplanetary mission. The interested reader can refer to the Introduction section of reference [28] to obtain a snapshot of the recent research concerning comet 29P/Schwassmann–Wachmann 1 (indicated as "comet SW1" in the rest of this paper). The current, heliocentric orbit of comet SW1 is nearly circular (the actual eccentricity is 4.4526×10^{-2}), with an inclination of about 9 deg. The comet orbit is between Jupiter and Saturn [29]. The numerical results discussed in reference [28] indicate that a simplified circle-to-circle, two-dimensional transfer scenario can be used to approximate the real, three-dimensional Earth–comet SW1 trajectory in a classical interplanetary rendezvous mission. In this context, the comet orbit around the Sun is considered circular, with radius $r_{\text{SW1}} = 6.0499$ AU, and coplanar to the heliocentric (assumed circular with radius $r_0 = 1$ AU) orbit of Earth.

Therefore, in this heliocentric scenario (in which $\mu = \mu_\odot$), the dimensionless target radius is $\tilde{r}_f = r_{\text{SW1}}/r_0 = \tilde{r}_{\text{SW1}} = 6.0499$, and Equation (38) gives the function $n = n(\tilde{a}_m)$, sketched in Figure 4. According to Figure 4, the condition $n \geq 2$ is approximately satisfied when $\tilde{a}_m \leq 0.02$, so the optimal Earth–comet SW1 transfer is studied parametrically considering (again) a dimensionless maximum propulsive acceleration in the range $\tilde{a}_m \in [0.001, 0.02]$. Note that, in this case, one has $\mu_\odot/r_0^2 \simeq 5.93\,\text{mm/s}^2$ so that a value $\tilde{a}_m = 0.02$ (or $\tilde{a}_m = 0.001$) corresponds to a dimensional propulsive acceleration of $0.1186\,\text{mm/s}^2$ (or $0.00593\,\text{mm/s}^2$).

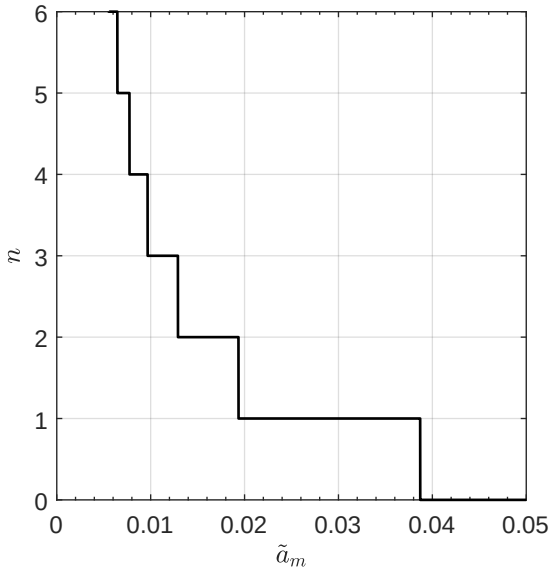

Figure 4. Earth–comet SW1 scenario: number n of completed revolutions around the Sun as a function of $\tilde{a}_m$; see also Equation (38).

The TPBVP associated with the optimization problem was solved using the procedure previously described, and the results of the numerical simulations are summarized in Table 5, which can be considered as an extension (to this scenario) of the results of Tables 1–4. As expected, the values in Table 5 confirm the accuracy of the proposed analytical model based on Equations (26), (29), and (33).

Table 5. Results of the numerical simulations in the Earth–comet SW1 transfer mission scenario.

$\tilde{a}_m$	$\tilde{t}_f$	$\frac{\theta(\tilde{t}_f)}{2\pi\ \mathrm{rad}}$	n	R_t	R_δ	R_λ
0.0200	40.3294	2.1369	1	0.7357	1.0087	0.8705
0.0190	42.1231	2.2439	2	0.7415	1.0652	0.9147
0.0180	44.0030	2.3658	2	0.7492	1.0899	1.0108
0.0170	45.9338	2.5002	2	0.7600	1.0538	1.1162
0.0160	47.9743	2.6413	2	0.7731	0.9825	1.1510
0.0150	50.2988	2.7910	2	0.7866	0.9263	1.0768
0.0140	53.1727	2.9631	2	0.7972	0.9279	0.9401
0.0130	56.7861	3.1749	2	0.8039	1.0191	0.8893
0.0120	60.8125	3.4373	3	0.8132	1.0741	1.0500
0.0110	65.0024	3.7288	3	0.8300	0.9561	1.1133
0.0100	70.4270	4.0626	3	0.8426	0.9618	0.9048
0.0090	77.3320	4.5097	4	0.8527	1.0531	1.0836
0.0080	85.2293	5.0274	4	0.8704	0.9498	0.9276
0.0070	95.8565	5.7316	5	0.8844	0.9679	1.1042
0.0060	109.9957	6.6533	6	0.8992	1.0015	1.1110
0.0050	129.3736	7.9270	7	0.9174	0.9398	0.9999
0.0040	158.7425	9.8625	9	0.9346	0.9480	1.0416
0.0030	207.6458	13.0749	12	0.9526	0.9647	0.9397
0.0020	305.6158	19.5310	19	0.9709	1.0429	1.0400
0.0010	599.4593	38.8484	38	0.9900	0.9746	1.0404

The time variation in the thrust angle and the corresponding optimal transfer trajectory are two outputs of the optimization process. Assuming, for example, $\tilde{a}_m = \{0.001, 0.005, 0.01, 0.02\}$, the polar form of the optimal transfer trajectory is sketched in Figure 5, while the (dimensionless) time variation in the thrust angle α is shown in Figure 6. Note that, according to Figure 6, when the magnitude of the propulsive acceleration is sufficiently low (as in the case of $\tilde{a}_m = 0.001$), the value of the thrust angle during the entire transfer is close to $\pi/2$ rad, as modeled by

Equation (25). However, when the value of $\tilde{a}_m$ increases (or the primary body–spacecraft distance is high, as at the end of the transfer), the thrust angle diverges from the value predicted by Equation (25). In any case, the initial value of α, which coincides with the auxiliary angle δ, is roughly equal to $\pi/2$ rad, as expected.

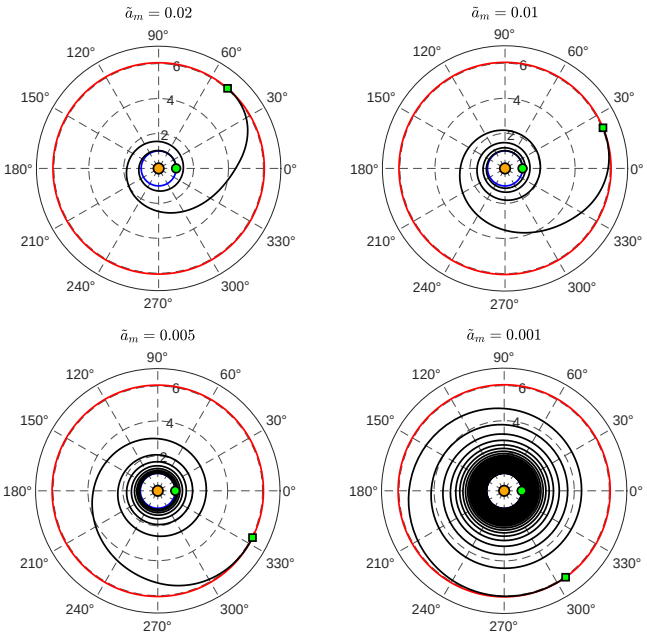

Figure 5. Optimal transfer trajectory in an Earth–comet SW1 mission scenario, as a function of $\tilde{a}_m = \{0.001, 0.005, 0.01, 0.02\}$. Black line → transfer trajectory; blue line → Earth (parking) orbit; red line → comet SW1 (target) orbit; green circle → start point; green square → arrival point; orange circle → Sun. Radial distances are in astronomical units.

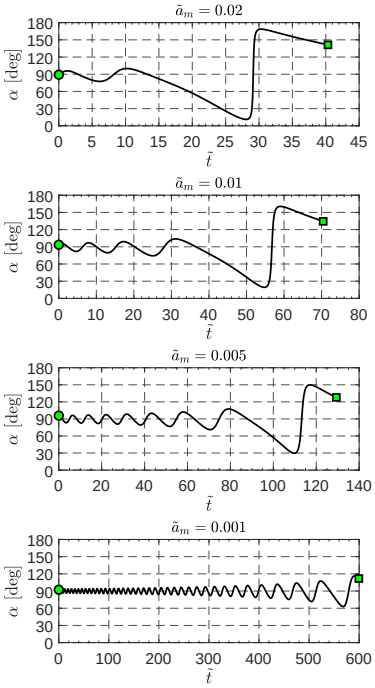

Figure 6. Optimal time variation in the thrust angle α in an Earth–comet SW1 mission scenario, as a function of $\tilde{a}_m = \{0.001, 0.005, 0.01, 0.02\}$. Green circle → start point; green square → arrival point.

6. Conclusions

In this paper, we studied the transfer between two circular, coplanar orbits of assigned characteristics, considering a spacecraft operated with a continuous thrust propulsion system that provides a magnitude of propulsive acceleration vector within an assigned range. The problem is addressed in an optimal framework using a classical indirect approach, minimizing the total flight time as a function of the target orbit radius and the characteristics of the propulsion system. The main contribution of this work is to use a simplified version of the spacecraft dynamics, not to approximate the (optimal) transfer trajectory but to accurately estimate the initial value of the unknown costates needed to solve the TPBVP associated with the optimization process.

The proposed procedure allows the initialization of the TPBVP with a guessed solution reasonably close to the actual one determined through a numerical approach based on the classic single shooting method. The method is designed to work well when the maximum magnitude of the propulsive acceleration vector is sufficiently small when compared with the gravitational acceleration of the primary body along the circular parking orbit. However, the procedure can still be used when the value of the propulsive acceleration is medium–high, in order to obtain a rough estimate of the initial costates. In this regard, the availability of a set of analytical equations, such as the one presented in this paper, is a useful (and important) tool in the preliminary phase of mission design.

Funding: This research received no external funding.

Institutional Review Board Statement: Not applicable.

Informed Consent Statement: Not applicable.

Data Availability Statement: Data are contained within the article.

Conflicts of Interest: The author declares no conflicts of interest.

Abbreviations

The following abbreviations are used in this manuscript:

$\boldsymbol{a}_p$	propulsive acceleration vector, with $a_p = \|\boldsymbol{a}_p\|$
a_m	maximum value of the propulsive acceleration magnitude a_p
$\mathcal{H}$	Hamiltonian function
$\mathcal{H}_c$	part of the Hamiltonian which depends on the controls
$\hat{\boldsymbol{i}}_r$	radial unit vector
$\hat{\boldsymbol{i}}_\theta$	transverse unit vector
J	performance index to be maximized
n	number of complete revolutions around the primary body
O	primary body center-of-mass
$\{R_t, R_\delta, R_\lambda\}$	dimensionless ratio; see Equation (39)
r	radial distance
S	spacecraft center-of-mass
t	time
$\mathcal{T}$	polar reference frame
u	radial component of the spacecraft velocity
v	transverse component of the spacecraft velocity
α	thrust angle
δ	auxiliary angle
Δt	flight time
ΔV	accumulated velocity change
θ	spacecraft polar angle
$\lambda_{\tilde{r}}$	costate of $\tilde{r}$
$\lambda_{\tilde{u}}$	costate of $\tilde{u}$

$\lambda_{\tilde{v}}$	costate of $\tilde{v}$
λ_{θ}	costate of θ
μ	primary body gravitational parameter
Subscripts	
0	initial, circular parking orbit
an	evaluated through analytical approximation
f	final, circular target orbit
G	geocentric mission scenario
GEO	geostationary orbit
LEO	low-Earth orbit
num	numerically evaluated
$\oplus$	Earth
♃	Jupiter, Jupiter-based scenario
♂	Mars, Mars-based scenario
$\odot$	Sun
♀	Venus, Venus-based scenario
Superscripts	
$\cdot$	derivative with respect to t
$'$	derivative with respect to $\tilde{t}$
$\sim$	dimensionless form

References

1. Gurfil, P. Spacecraft Rendezvous Using Constant-Magnitude Low Thrust. *J. Guid. Control. Dyn.* **2023**, *46*, 2183–2191. [CrossRef]
2. Bryson, A.E.; Ho, Y.C. *Applied Optimal Control*; Hemisphere Publishing Corporation: New York, NY, USA, 1975; pp. 66–89; Chapter 2.
3. Betts, J.T. Survey of Numerical Methods for Trajectory Optimization. *J. Guid. Control. Dyn.* **1998**, *21*, 193–207. [CrossRef]
4. Conway, B.A. A Survey of Methods Available for the Numerical Optimization of Continuous Dynamic Systems. *J. Optim. Theory Appl.* **2011**, *152*, 271–306. [CrossRef]
5. Stengel, R.F. *Optimal Control and Estimation*; Dover Books on Mathematics; Dover Publications, Inc.: New York, NY, USA, 1994; pp. 222–254.
6. Zhao, S.; Gurfil, P.; Zhang, J. Initial Costates for Low-Thrust Minimum-Time Station Change of Geostationary Satellites. *J. Guid. Control. Dyn.* **2016**, *39*, 2746–2756. [CrossRef]
7. Guo, X.; Wu, D.; Jiang, F. Minimum-Time Rendezvous via Simplified Initial Costate Normalization and Auxiliary Orbital Transfer. *J. Guid. Control. Dyn.* **2023**, *46*, 1627–1636. [CrossRef]
8. Alfano, S.; Thorne, J.D. Circle-to-Circle Constant-Thrust Orbit Raising. *J. Astronaut. Sci.* **1994**, *42*, 35–45.
9. Alfano, S.; Thorne, J.D. *Constant-Thrust Orbit-Raising Transfer Charts*; Technical Report PL-TR-93-1010; Phillips Laboratory, Space and Missiles Technology Directorate, Kirtland Air Force Base: Albuquerque, NM, USA, 1993. Available online: https://apps.dtic.mil/sti/citations/ADA269088 (accessed on 15 December 2023)
10. Wiesel, E.E.; Alfano, S. Optimal Many-Revolution Orbit Transfer. *J. Guid. Control. Dyn.* **1985**, *8*, 155–157. [CrossRef]
11. Bacon, R.H. Logarithmic spiral: an ideal trajectory for the interplanetary vehicle with engines of low sustained thrust. *Am. J. Phys.* **1959**, *27*, 164–165. [CrossRef]
12. Bassetto, M.; Quarta, A.A.; Mengali, G. Analytical solution to logarithmic spiral trajectories with circumferential thrust and mission applications. *Astrodynamics* **2022**, *6*, 413–427. [CrossRef]
13. Huang, S.; Colombo, C.; Bernelli-Zazzera, F. Low-thrust planar transfer for co-planar low Earth orbit satellites considering self-induced collision avoidance. *Aerosp. Sci. Technol.* **2020**, *106*, 106198. [CrossRef]
14. Gong, S.; Macdonald, M. Review on solar sail technology. *Astrodynamics* **2019**, *3*, 93–125. [CrossRef]
15. Fu, B.; Sperber, E.; Eke, F. Solar sail technology—A state of the art review. *Prog. Aerosp. Sci.* **2016**, *86*, 1–19. [CrossRef]
16. Janhunen, P.; Toivanen, P.K.; Polkko, J.; Merikallio, S.; Salminen, P.; Haeggström, E.; Seppänen, H.; Kurppa, R.; Ukkonen, J.; Kiprich, S. Electric solar wind sail: Toward test missions. *Rev. Sci. Instrum.* **2010**, *81*, 111301. [CrossRef]
17. Bassetto, M.; Niccolai, L.; Quarta, A.A.; Mengali, G. A comprehensive review of electric solar wind sail concept and its applications. *Prog. Aerosp. Sci.* **2022**, *128*, 100768. [CrossRef]
18. Ross, I.M. *A Primer on Pontryagin's Principle in Optimal Control*; Collegiate Publishers: San Francisco, CA, USA, 2015; Chapter 2, pp. 127–129.
19. Lawden, D.F. *Optimal Trajectories for Space Navigation*; Butterworths & Co.: London, UK, 1963; pp. 54–60.
20. Yang, W.Y.; Cao, W.; Kim, J.; Park, K.W.; Park, H.H.; Joung, J.; Ro, J.S.; Hong, C.H.; Im, T. *Applied Numerical Methods Using MATLAB®*; John Wiley & Sons, Inc.: Hoboken, NJ, USA, 2020; Chapters 6 and 7, pp. 333–336.
21. Quarta, A.A.; Mengali, G. Semi-Analytical Method for the Analysis of Solar Sail Heliocentric Orbit Raising. *J. Guid. Control. Dyn.* **2012**, *35*, 330–335. [CrossRef]

22. Bassetto, M.; Quarta, A.A.; Caruso, A.; Mengali, G. Optimal heliocentric transfers of a Sun-facing heliogyro. *Aerosp. Sci. Technol.* **2021**, *119*, 107094. [CrossRef]
23. Shampine, L.F.; Reichelt, M.W. The MATLAB ODE Suite. *SIAM J. Sci. Comput.* **1997**, *18*, 6424. [CrossRef]
24. Sarid, G.; Volk, K.; Steckloff, J.; Harris, W.; Womack, M.; Woodney, L. 29P/Schwassmann-Wachmann 1, A Centaur in the Gateway to the Jupiter-family Comets. *Astrophys. J. Lett.* **2019**, *883*, 25. [CrossRef]
25. Betzler, A.S. A photometric study of centaurs 29P/Schwassmann-Wachmann and (2060) Chiron. *Mon. Not. R. Astron. Soc.* **2023**, *523*, 3678–3688. [CrossRef]
26. Kokhirova, G.; Ivanova, O.; Rakhmatullaeva, F.D.; Buriev, A.; Khamroev, U. Astrometric and photometric observations of comet 29P/Schwassmann-Wachmann 1 at the Sanglokh international astronomical observatory. *Planet. Space Sci.* **2020**, *181*, 104794. [CrossRef]
27. Picazzio, E.; Luk'yanyk, I.V.; Ivanova, O.V.; Zubko, E.; Cavichia, O.; Videen, G.; Andrievsky, S.M. Comet 29P/Schwassmann-Wachmann 1 dust environment from photometric observation at the SOAR Telescope. *Icarus* **2019**, *319*, 58–67. [CrossRef]
28. Quarta, A.A.; Abu Salem, K.; Palaia, G. Solar sail transfer trajectory design for comet 29P/Schwassmann-Wachmann 1 rendezvous. *Appl. Sci.* **2023**, *13*, 9590. [CrossRef]
29. Neslusan, L.; Tomko, D.; Ivanova, O. On the chaotic orbit of comet 29P/Schwassmann-Wachmann 1. *Contrib. Astron. Obs. Skaln. Pleso* **2017**, *47*, 7–18.